



# 1        **A Wavelength Dispersive Instrument for Characterizing Fluorescence and** 2        **Scattering Spectra of Individual Aerosol Particles on a Substrate**

3  
4        Donald R. Huffman<sup>1</sup>, Benjamin E. Swanson<sup>2</sup>, and J. Alex Huffman<sup>2\*</sup>

5  
6        <sup>1</sup> University of Arizona, Department of Physics, Tucson, Arizona

7        <sup>2</sup> University of Denver, Department of Chemistry and Biochemistry, Denver, Colorado

8  
9        \* *Correspondence to:* J. Alex Huffman ([alex.huffman@du.edu](mailto:alex.huffman@du.edu))

10  
11  
12        **Abstract:** We describe a novel, low-cost instrument to acquire both elastic and inelastic  
13        (fluorescent) scattering spectra from individual micron-size particles in a multi-particle  
14        collection on a microscope slide. The principle of the device is based on a slitless spectroscope  
15        often employed in astronomy to determine the spectra of individual stars in a star cluster, but that  
16        had not been applied to atmospheric particles. Under excitation, most commonly by either a 405  
17        nm diode laser or a UV light emitting diode (LED), fluorescent emission spectra of many  
18        individual particles can be determined simultaneously. The instrument can also acquire elastic  
19        scattering spectra from particles illuminated by a white light source. Advantages and  
20        disadvantages of using black-and-white cameras compared to color cameras are given. The  
21        primary motivation for this work has been to develop an inexpensive technique to characterize  
22        fluorescent biological aerosol particles. An example of an iPhone-enabled device is also shown  
23        as a means for collecting data on biological aerosols at lower cost or utilizing citizen scientists  
24        for expanded data collection.

## 25        1. Introduction

26        Primary biological aerosol particles (PBAP) suspended in the atmosphere, often termed  
27        bioaerosols, are comprised of a complex mixture of biological organisms and materials including  
28        bacteria, fungal spores, pollen, and fragments and excretions of plants, animals, and  
29        microorganisms (Després et al., 2012). They can influence human, animal, and agricultural  
30        health by causing disease and triggering allergies, and can influence Earth systems such as cloud  
31        formation and the hydrological cycle by acting as nuclei for the formation of liquid water or ice  
32        cloud droplets (Douwes et al., 2003; Möhler et al., 2007; Morris et al., 2014; Pöschl et al., 2010;  
33        Pöschl and Shiraiwa, 2015). Yet large holes in the collective understanding about atmospheric  
34        bioaerosols remain, and PBAP have become increasingly important in recent years in aerosol  
35        science due to synergistic advancements in detection technologies and in the understanding of  
36        roles these aerosols may play in the atmospheric system.

37  
38        One common method for the discrimination of biological particles from the rest of atmospheric  
39        particulate matter is the use of single-particle laser-induced fluorescence (LIF). Many research  
40        groups have utilized LIF for real-time investigation of bioaerosols, often for the purpose of  
41        detecting possible agents of bioterrorism (e.g. Després et al., 2012; Kiselev et al., 2011;  
42        Manninen et al., 2008; Pan et al., 2003; Pan et al., 2010; Saari et al., 2014; Sivaprakasam et al.,  
43        2004; Sivaprakasam et al., 2009). Over the last 10-15 years a number of LIF instruments have  
44        also become commercially available and are becoming more widely used for atmospheric  
45        research. Two of the bioaerosol-LIF instruments most commonly used within the atmospheric



46 research community are the ultraviolet aerodynamic particle sizer (UV-APS; TSI, Inc.,  
47 Shoreview, MN) (Hairston et al., 1997; Huffman et al., 2010) and the wideband integrated  
48 bioaerosol sizer (WIBS; DMT, Inc., Boulder, CO) (Foot et al., 2008; Gabey et al., 2010; Kaye et  
49 al., 2005; Perring et al., 2015). Both instruments allow characterization of particles with high  
50 time- and size-resolution, but offer little spectral discrimination. The UV-APS provides  
51 aerodynamic particle size-resolved information about ensembles of particles averaged for several  
52 seconds or minutes, and fluorescence excited at 355 nm is provided as the sample-average  
53 emission intensity in one wavelength band between 420 – 575 nm (Hairston et al., 1997). The  
54 WIBS provides optical particle size and fluorescence information for each particle interrogated,  
55 using two excitation wavelengths of 280 nm and 370 nm, and detects fluorescence emission in 2  
56 channels for each excitation (Foot et al., 2008). Further, both instruments are quite expensive,  
57 selling for approx. \$100k or more. The poor spectral resolution limits the ability of these  
58 instruments to finely discriminate between particle types, and the high cost of these instruments  
59 prevents their widespread global application.

60  
61 If instruments of considerably less cost and smaller size could be developed and distributed with  
62 the capability to discriminate biological particles from non-biological material, the information  
63 on the global properties of biological aerosol particles and their effect on human health and  
64 climate could be collected on a much more comprehensive scale. We have developed a low-cost  
65 instrument capable of characterizing fluorescence and white-light spectra from many individual  
66 particles collected onto a substrate, each excited at several excitation wavelengths. Here we  
67 introduce both a benchtop and a portable, smartphone-based instrument that each may serve as a  
68 transformative tool for bioaerosol detection with application to atmospheric research, pollen  
69 monitoring, and mold spore detection, among many other applications. The instrument design  
70 also has potential application to any scientific or medical problem where a minority of micron-  
71 sized particles can be discriminated from a majority of particles based on their fluorescence or  
72 elastic scattering spectra.

## 73 2. Instrument description

74 The instrument is built around a conventional compound microscope and uses standard glass  
75 microscope slides as particle substrates, though any non-fluorescent and relatively non-reflective  
76 material may be utilized. We will explain the principle and the details with reference to a three-  
77 stage progression of the idea as shown in Figure 1. The optical principle is derived from the  
78 simple spectroscope as shown in Figure 1a. In this venerable instrument, the light to be spectrally  
79 analyzed is directed onto a narrow incident slit. The light from this slit is made parallel by the  
80 collimating lens and impinges on a wavelength-dispersive element such as a prism or a  
81 transmission grating (as shown). Parallel light from the grating is dispersed into an angle  $\theta$  by  
82 the grating according to the grating equation for normal incidence (Jenkins and White, 1957),

$$83 \quad d \sin \theta = n\lambda \quad (1)$$

84 where  $d$  is the distance between rulings on the grating,  $n$  is an integer giving the order of  
85 diffraction, and  $\lambda$  is the wavelength of the light. For the example in Figure 1a an atomic emission  
86 source such as H, He, or Hg is shown as the light source, which illuminates a narrow slit from  
87 behind. An image of the slit at each wavelength is dispersed according to the angle defined in  
88 Equation 1. Because there are multiple wavelengths emitted in the visible region by the sources  
89 just mentioned, there will be a real image of the slit, which gives rise to the “line spectrum” that



90 can be viewed with an eyepiece. This real image can also be captured on photographic film or on  
91 an array detector such as a charge-coupled device (CCD) or complementary metal-oxide  
92 semiconductor (CMOS) detector in a digital camera.

93  
94 The essential innovation of the present instrument is understood by imagining the replacement of  
95 the back-illuminated slit by one or more particles in place of the slit, held on the plane of a  
96 microscope slide as in Figure 1b. For detection at a  $\theta$  angle of zero (viewing straight through),  
97 the dark-field image appears simply as a collection of illuminated particles, and no spectral  
98 information is gained. Viewed at an appropriate angle through the transmission grating, however,  
99 the individual particles will exhibit spectral dispersion. For monochromatic illumination of a  
100 given particle, such as by a single spectral line or a laser beam, the first order diffraction will be  
101 a single spot imaged in the same plane that the slit image was shown previously. In the version  
102 shown in Figure 1b, however, the image at the detector will be located at vertical and horizontal  
103 coordinates corresponding to an image of the particle's position on the substrate. For white light  
104 illumination the dispersed image of each particle will be a swath of light with a height  
105 corresponding to the diameter of the particle and a length corresponding to the difference in  
106 dispersion angle for visible wavelengths. Each particle will display the various rainbows of  
107 colors when viewed by eye through an eyepiece. If the substrate consists of a number of particles  
108 distributed sparsely on the surface of a microscope slide as shown in Figure 1b, each particle will  
109 be imaged as either a single, colored point for illumination by a monochromatic source, a series  
110 of different colored points for a multiple line emission source, or a continuum spectrum for white  
111 light illumination.

112  
113 The main idea here is the replacement of an entrance slit, which is present in most spectroscopes  
114 and the spectrographs, monochromators, and spectrometers built upon the spectroscope idea of  
115 Figure 1a, with individual small particles each of which effectively act as very small (two-  
116 dimensional) slits as in Figure 1b. Thus this instrument falls into the category of a slitless  
117 spectrometer, which has been used widely, but mostly in astronomical studies. In the 1880's  
118 Edward Pickering implemented the idea by placing a large prism in front of the objective lens of  
119 a refracting telescope and recording the spectral swaths on photographic film for analysis (Hale  
120 and Wadsworth, 1896). In his classic textbook George Abell (1969) has shown images of the  
121 color spectra from all stars in the famous Pleiades star cluster in one image. With this as  
122 inspiration, we produced the spectral streaks from microscopic particles that look very much like  
123 the streaks from stars through a telescope.

124  
125 The incarnation of the instrument described here is relatively simple, yet has not been applied for  
126 aerosol particle research. Other commonly applied techniques provide aspects of the benefits  
127 described here, but are yet distinctly different (Lakowicz, 2010). Fluorescence microscopy is  
128 widely applied in many scientific fields, but most commercial fluorescence microscopes provide  
129 fluorescence information by utilizing relatively broad-wavelength filters for excitation and  
130 emission. As a result, micrographs can be achieved that utilize a given pair of excitation and  
131 emission windows, but spectral information can only be attained by using a large sequence of  
132 filters. Laser-scanning confocal microscopy allows the user to excite a given spot with a chosen  
133 laser source and then measure the spectral dependence of the fluorescent emission, but scanning  
134 a collection of particles can be time-consuming, because the laser must raster-scan through the  
135 entire field of view, and the instrumentation is costly and relatively complicated. Fluorescence



136 spectroscopy is achieved in the bulk phase, most often for solutions and suspensions, but is also  
137 possible for powders and solid materials, by measuring fluorescence emission spectra as the  
138 excitation wavelength is varied. In this case, highly resolved fluorescence emission spectra can  
139 be acquired, though fine spatial resolution is typically not possible and thus the technique  
140 typically cannot provide single particle spectra. Single-particle fluorescence instruments, such as  
141 are used for detection of atmospheric bioaerosols, normally provide very poor spectral resolution  
142 (total of 1-3 emission channels) and are very expensive (Foot et al., 2008; Hairston et al., 1997;  
143 Manninen et al., 2008; Sivaprakasam et al., 2004). A notable exception to the statement about  
144 spectral resolution is the single particle fluorescence spectrometer (SPFS) developed by the  
145 Army Research Laboratory (Pan et al., 2011; Pan et al., 2010). This instrument can provide  
146 highly resolved spectra of individual aerosol particles suspended in air flowing through the  
147 device, however, the instrument is one-of-a-kind and is very expensive (\$100k's). Thus, the  
148 instrument described here combines benefits of each of these other instrument concepts by  
149 delivering spectra of each particle in a collection on a substrate, each at a number of excitation  
150 wavelengths, and at a cost orders of magnitude lower than other techniques. Recently a similar  
151 concept of slitless microscope spectroscopy was used with silver nanoprobe applied to in vivo  
152 monitoring (Cheng et al., 2010; Xiong et al., 2013). This appears to have been the first  
153 application of slitless spectroscopy to single particles, however, the application was towards  
154 biomedical testing with no application to atmospheric aerosols and not towards a portable device.

### 155 *2.1 Typical operation*

156 Figure 1c adds some practical details about the instrument described here, the original of which  
157 was constructed from a student microscope (Model 656/98, SWIFT Microscopy, Carlsbad, CA)  
158 formerly used in an undergraduate biology teaching lab. The original vertical microscope was  
159 placed in a horizontal orientation, with the sample slide illuminated by one of several light  
160 sources consisting of diode lasers, LEDs, or a tungsten filament light bulb. Illumination of the  
161 particles from above and to the side of the stage produces a bright particle image on a dark  
162 background - one example of so-called dark field illumination. The microscope stage with its  
163 attached x-y positioner and the objective lens turret were retained from the original microscope.  
164 The eyepiece was removed and placed on a rail that rotates about a pivot point located in the  
165 plane of the transmission diffraction grating (300 grooves/mm; Thor Labs, Inc., GT25-03). A  
166 standard optical table with mounting holes spaced on a one inch grid supports optical rails and  
167 holders secured to it for mounting the optical components (Thor Labs, Inc.). Various cameras,  
168 both color and black and white (b/w) have been adapted with mounts to the rotating detector  
169 arm.

170  
171 In operation, when the camera arm is set at zero degrees, the instrument operates as a standard  
172 microscope. At the approximate angle of first order diffraction the camera will record spectral  
173 swaths of each particle in the field of view. We note that either elastic scattering (no change in  
174 wavelength upon scattering) or inelastic scattering (change of wavelength upon scattering) can  
175 be recorded. In all cases discussed in this paper inelastic scattering is due to fluorescence, though  
176 the concept will apply to inelastic Raman scattering, for example, and this will be investigated in  
177 future research. Thus the instrument has the capability of recording either elastic or inelastic  
178 scattering from individual particles in its field of view (of the order of one mm), depending on  
179 the type of particle and the illumination source. As a practical matter, the density of particles  
180 distributed on the slide should be sufficiently sparse that the spectral swaths do not overlap if  
181 individual particle spectra are to be determined. An additional optical element necessary for



182 fluorescence spectroscopy is a long-pass blocking filter which we place between the objective  
183 lens and the grating, selected so as to block the emission of the fluorescence-exciting source, but  
184 transmit the fluorescence spectrum to a wavelength as close as possible to the blocked laser  
185 wavelength. For example, we commonly use a diode laser with a wavelength of about 405 nm  
186 and long-pass filters chosen to block wavelengths below approx. 420 or 440 nm (Edmund  
187 Optics, 832916-10). We have also used 280, 370, and 450 nm excitation sources, but the process  
188 and concept remains the same.

## 189 **2.2 Example spectra and data analysis**

190 Individual panels of Figure 2 (a through d) serve to illustrate the different types of images  
191 collected during standard operation. Each panel of Figure 2 shows a sample of paper mulberry  
192 pollen (*Broussonetia papyrifera*; 12-13  $\mu\text{m}$ ; Allergon, SKU 0578) collected onto a conventional  
193 microscope slide after aerosolization by blowing air into a tube of pollen. Figure 2a shows pollen  
194 grains illuminated with red laser light and imaged as a standard micrograph, with the camera arm  
195 at zero degrees. Figure 2b is taken with illumination by the red and violet lasers simultaneously  
196 (wavelengths 650 nm and 405 nm, respectively). Dots on the left and right of each streak  
197 correspond to monochromatic images of the particles illuminated by the red and violet lasers,  
198 respectively. These appear as washed-out dots devoid of much color and large in size, as a result  
199 of the intensity of the illuminating lasers which saturate the detector. The swaths of color  
200 between the dots are due to fluorescence induced from the pollen particles. It should be noted  
201 that each of the spectral streaks in Figures 2b through 2d can be related to specific particles by  
202 way of their images in Figure 2a. Figure 2c shows an example white-light scattering spectra after  
203 illumination by a polychromatic tungsten filament. Figure 2d shows an identical image to that of  
204 Figure 2b, but without the red laser and with the blocking filter in place. In this way, the  
205 fluorescence spectra can be detected more sensitively, without wash-out from the red and violet  
206 lasers. By comparing Figures 2c and 2d one can see that the relative fraction of pollen particles  
207 fluorescent in this sample is nearly 100%, since this particulate sample is made up of a single  
208 kind of pollen.

209  
210 Two laser spots of known wavelength give the ability to calibrate the pixel location with respect  
211 to wavelength for each of the spectral swaths. The wavelength scale for each particle is  
212 established by determining the wavelength dispersion from the positions in pixel numbers of the  
213 red and violet calibration spots, assuming a linear dependence of wavelength on distance in the  
214 plane of focus. Making use of the open source program suite Image J (Rasband, 1997) one draws  
215 a box in the region of interest closely around the spectral swath. Employing the program's ability  
216 to determine average intensity at each horizontal pixel location on the swath, the data is  
217 presented in two columns – one column corresponding to horizontal pixel number and the other  
218 column corresponding to average light intensity detected at the given pixel number. These data  
219 columns are entered into a spread sheet and the pixel numbers are converted to a column of  
220 wavelength values using the dispersion calibration already determined.

221  
222 Figure 3 shows the normalized fluorescence spectrum of three particles from the fluorescence  
223 image in Figure 2d acquired by determining the intensity as a function of wavelength, as  
224 discussed above. The result is a broad peak centered at approx. 500 nm, broadly consistent with  
225 previous literature for many types of pollen (Hill et al., 2009; Pan et al., 2011; Pöhlker et al.,  
226 2013; Pöhlker et al., 2012). A secondary peak, caused by the color camera pixels centered at  
227 approx. 600 nm, is also clear and will be discussed in a following section.



### 228 3. Applications

229 In Figure 4 we present images for two different collections of particles that highlight the simplest  
230 application of the instrument, which is to estimate the fraction of particles in a mixture that  
231 exhibit fluorescence. This can be achieved irrespective of whether emission spectra are  
232 measured, and can have important application to a number of scientific questions. For example,  
233 the UV-APS has been frequently applied to the detection of bioaerosols in ambient air (Huffman  
234 et al., 2010), but it cannot provide spectrally resolved information and thus essentially only  
235 provides information about the fraction of particles that exhibit fluorescence at a given set of  
236 excitation and emission wavelengths. Figure 4 shows images associated with particulate samples  
237 of polydisperse particle size, as opposed to those shown in Figure 2 which are very uniform in  
238 size.

#### 239 3.1 Outdoor sample particles

240 The particles shown in Figures 4a-c (top panel) were collected by leaving a glass microscope  
241 slide lying horizontally on a table three feet above ground level outdoors in Tucson, Arizona for  
242 24 hours in the winter time in clear weather. The comparison of the fluorescence image (Fig. 4c)  
243 with the elastic scattering image (Fig. 4b) is an illustration that the fraction of aerosol particles  
244 exhibiting fluorescence is relatively easily achieved without needing to analyze spectra and thus  
245 with little image processing. In fact, a rough idea about the relative fluorescent fraction can be  
246 achieved by eye simply by looking at camera images using both illumination schemes (e.g. Figs.  
247 4b-c). The count for elastic scattering particles, which should comprise all particles both  
248 fluorescent and non-fluorescent, is approx. 46 in this example, whereas the number count of the  
249 brightly fluorescent particles is approx. 7. Thus the fraction of total particles that are fluorescent,  
250 and presumably of biological origin, is approx.  $7/46$  here or approx. 9%, which is broadly  
251 consistent with typical ambient measurements, though fluorescent biological aerosol  
252 concentrations and properties vary widely by season and geography (Huffman et al., 2013;  
253 Schumacher et al., 2013). This fraction is also highly dependent on the threshold one applies to  
254 categorize a given particle as fluorescent or not, and fluorescence intensity is strongly a function  
255 of particle size. Most fluorescence-based aerosol detectors are faced with this difficult challenge  
256 of categorization, and the sensitivity of a given detector will significantly influence the  
257 comparison of the relative fraction of fluorescent particles detected by any two instruments or  
258 types of instruments (Healy et al., 2014; Hernandez et al., 2016; Huffman et al., 2012; Saari et  
259 al., 2013).

#### 260 3.2 Fused silica particles

261 For the purpose of illustrating results for a particle collection expected to show no fluorescence  
262 we prepared a collection of particles by grinding a piece of optical fused silica with an agate  
263 mortar and pestle. The optical silica of the starting material shows no appreciable fluorescence in  
264 bulk throughout the visible spectral region. A large spread of particle sizes is apparent in the  
265 micrograph of Figure 4d with many overlapping elastic scattering spectra, apparent under  
266 illumination with the white light of a tungsten lamp (Fig. 4e). Figure 4f, however, shows one  
267 unexpected, strongly fluorescent particle and approximately three other weakly fluorescent  
268 particles. The elastic scattering (Fig. 4e) for these particles is not particularly remarkable. Our  
269 interpretation is that the very few fluorescent particles observed are contaminants of fluorescent  
270 material, which entered into the mixture during grinding or handling in a relatively dirty  
271 laboratory, and which had previously contained various pollen particles. We refer to the image



272 series in Figure 4d-f as “a fluorescent needle in an elastic scattering haystack.” It illustrates how  
273 biological impurities might easily be detected with our apparatus even in the presence of a large  
274 majority of non-biological, or otherwise non-fluorescent particles.

#### 275 **4. Comparison of black-and-white with color cameras**

276 Results presented to this point have been based on images taken using a Canon Powershot  
277 A2300 HD color camera, which is a simple point-and-shoot digital camera costing less than  
278 \$100. It was chosen to promote the goal of producing a relatively low cost apparatus. We have  
279 also used a more sophisticated black and white (b/w) or monochrome camera – a Luminara  
280 Infinity 2-1R costing about \$2000. Color cameras in general have several disadvantages  
281 compared to b/w cameras, as well as some advantages. They use CCD or CMOS detector arrays  
282 with three different color pixels and filters having peak sensitivities in (for example) the red,  
283 green, and blue. When a broad continuum of light is incident on such a detector, as from a  
284 tungsten lamp or a broadband fluorescence spectrum from a pollen grain, the otherwise smooth  
285 spectral curve will show variations due to the color pixel characteristics. Figure 5 shows this  
286 effect experimentally with the white light spectrum from an incandescent tungsten-filament bulb  
287 (General Electric, Miniature Lamp 210, B6, 6.5V) scattered from ground particles of sodium  
288 chloride (NaCl; Sigma Aldrich, CAS# 7647-14-5) and independently detected by the  
289 monochrome camera and color camera discussed above. Each NaCl particle is expected to  
290 exhibit reasonably smooth scattering vs. wavelength, because its large size relative to the  
291 wavelength and its irregular shape do not promote the various sphere-like resonances expected  
292 from Mie theory (Bohren and Huffman, 1983). The monochrome camera yields a relatively  
293 smooth, broad scattering curve. For comparison, Figure 5 also shows the emission spectrum from  
294 a 3000 Kelvin blackbody multiplied by the theoretical sensitivity curve of the CCD used in the  
295 monochrome camera<sup>1</sup>. The theoretical blackbody curve and the measured elastic scattering curve  
296 match closely, suggesting that the monochrome camera introduces very little aberration as a  
297 function of wavelength. In contrast, the color camera shows a spectrum with pronounced peaks  
298 that are due to the different color pixels. These strong variations in the spectra from color  
299 cameras are difficult to correct for and are not present in monochrome cameras. Another  
300 disadvantage of most color cameras is the incorporation of an infrared blocking filter which is  
301 added to exclude light of wavelengths longer than deep red in order to produce a more natural  
302 color in the image, but which limits the red spectral range of fluorescence and elastic scattering  
303 detection.

304  
305 To further illustrate both of these undesirable features of color cameras, Figure 6 shows a  
306 comparison of images from particles of Kentucky bluegrass pollen (*Poa praeensis*, also known  
307 as *smooth or common meadow-grass*; 20 - 120  $\mu\text{m}$ ; Allergon SKU 0116), recorded and analyzed  
308 as described above to derive the spectral curves from both the b/w (black curve) and the color  
309 camera (red curve). The b/w camera results show a broad fluorescence band peaking near 490  
310 nm and a somewhat narrower band near 680 nm. The latter band is assigned to chlorophyll-a,  
311 which is present in most grass pollens (Maxwell and Johnson, 2000; O'Connor et al., 2011;  
312 O'Connor et al., 2014). A reference spectrum of bulk bluegrass pollen powder was achieved by  
313 adding approx. 5 mg of pollen to one well of a black 96-well plate (Fisher Scientific, 07-200-  
314 329) and recording a fluorescence emission spectrum at 405 nm excitation using a microplate  
315 reader spectrofluorometer (Infinite M1000 Pro, Tecan, Männerdorf, Switzerland). This technique

<sup>1</sup> <http://www.opticstar-ccd.com/Images/Astronomy/Imagers/OS/Common/QE-ICX205AL-594x255.jpg>



316 cannot provide single-particle spectra, as discussed previously, but delivers a spectrum as an  
317 average of the bulk powder. The peak locations in the reference and b/w camera spectra are  
318 identical, though the relative ratio of chlorophyll peak to main peak is higher in the reference  
319 spectrum. This is expected, as individual pollen grains exhibit markedly different concentrations  
320 of chlorophyll as a result of differences in age and physiological state (Boyain-Goitia et al.,  
321 2003; Pöhlker et al., 2013). The color camera also shows a band near 490 nm as well as an  
322 irregular and asymmetric peak near 600 nm, with no sign of the chlorophyll band. The ~600 nm  
323 structure appears in the color camera image due to the color pixel effect discussed above. The  
324 absence of the chlorophyll peak from the color camera is likely due to the presence of the  
325 infrared blocking filter in the color camera only, which removes the transmission of chlorophyll  
326 transmission.

327

328 Notwithstanding the disadvantages of the color camera, it has several pleasant and useful  
329 features. First of all, the images of the spectra are simply interesting and beautiful! This may  
330 even be a non-trivial benefit when soliciting effort from citizen scientists, because the images  
331 can produce captivating, artistic views of the natural, microscopic world. From a practical  
332 scientific viewpoint, the colors are valuable for quickly getting oriented to the approximate  
333 wavelength positions of spectral features, which may be evident in the spectral swaths even  
334 without further processing. Also, the spectral colors are very useful when higher order spectra ( $n$   
335  $> 1$  in Equation 1) are present, which may result in overlapping orders. These can be easily  
336 sorted out if colored swaths are present, while they can become confusing when viewing the  
337 colorless black and gray images from a monochrome camera. For many investigations we have  
338 utilized both cameras in tandem, and perhaps the best solution in the future will be to use a  
339 combination of a b/w camera along with a color camera for standard usage. The two could be  
340 arranged on optical axes at 90 degrees from one another with a “flip mirror” used as a quick  
341 method to switch from one to the other.

## 342 **5. Smartphone embodiment**

343 Because of the development of smartphones for the vast, global consumer market, smartphones  
344 now contain highly sophisticated cameras built into the devices which are light-weight, low in  
345 electrical power, and relatively inexpensive. These devices also can have other useful capabilities  
346 such as GPS sensors providing geographic location, temperature and time detection, and the  
347 capability of connecting easily to the internet for almost immediate sharing of data. We built and  
348 tested two prototypes of the particle spectrometer – one for an iPhone and one for an Android  
349 phone. Figure 7a shows a photograph of the iPhone version, with an iPhone model 5s (Apple,  
350 Inc.) placed on top. The iPhone uses its own battery for the camera and other smartphone  
351 functions. Behind the wooden panels of the instrument body (13.3 x 13.3 x 7.4 cm; 58 g) are the  
352 same optical components discussed above regarding the benchtop version. There is an objective  
353 lens, blocking filter, and diffraction grating as well as three light sources (red and violet laser  
354 diodes and tungsten light source) operated by 2 AA batteries. The microscope slide onto which  
355 particles are collected can be slipped through a hole in the exterior casing, and four switches on  
356 the side of the instrument, attached to the anodized aluminum panel, operate the light sources so  
357 that images can be acquired without opening the case to ambient light. At present the little  
358 instrument only acquires and saves images, which must be downloaded to a computer for  
359 processing, as described earlier in this paper. A future goal is to utilize a combination of on-  
360 board and cloud-based image processing to provide spectra to the smartphone user.



361 The second panel (Figure 7b) shows a typical image of Kentucky bluegrass pollen taken with  
362 this instrument. The image shows fluorescence streaks from individual particles, similar to  
363 images acquired using the benchtop instrument (Fig. 2) as discussed above. Because of the wide  
364 angle of acceptance of the iPhone camera, the  $\Theta = 0$  microscope image is visible in the middle of  
365 the image as well as first order diffraction streaks to both the left and right. The fluorescence  
366 intensity of the right-most image is less than for the light diffracted to the left due to the blaze  
367 angle of the grating. The peak at  $\sim 600$  nm arises from the wavelength dependence of the color  
368 pixels, as discussed above. It is important to note here, however, that the peak at  $\sim 680$  nm shows  
369 the chlorophyll-a peak, in contrast to the absence of this peak when using the Canon color  
370 camera discussed previously.

## 371 **6. A vision for broad scale use**

372 Our vision for broad-scale use of a portable version of the instruments is twofold. First, the  
373 ability to sample and analyze fluorescence spectra of airborne particles has been limited because  
374 UV-LIF instruments are so expensive that they are typically deployed one at a time. This means  
375 that only in rare cases have such instruments been utilized to record information about  
376 bioaerosols to understand spatial variability. With the development of a sampler for particle  
377 collection hyphenated to the optical analysis tool described above, it could be possible for many  
378 units to be constructed inexpensively and deployed simultaneously, thus allowing for the  
379 collection and analysis of particles in a network across a chosen area. For this to become a reality  
380 we are working towards a future model which will incorporate automatic sampling and analysis  
381 capabilities, for example utilizing a Raspberry Pi camera to reduce the need for a dedicated  
382 smartphone for each unit.

383  
384 A second vision, specifically applicable to the smartphone version, is to involve interested  
385 citizen scientists from around the world who already possess the most expensive components of  
386 a fluorescent instrument – the smartphone camera. Our opto-mechanical additions to the smart  
387 phone meet the desired requirements of being relatively light weight, low power and  
388 inexpensive. At an estimated cost in bulk of about \$200, some 500 units (not counting the  
389 smartphone) could perhaps be produced for the approximately \$100,000 price of a real-time,  
390 commercial sensor such as the WBS. Interested persons could be enlisted to collect and measure  
391 particles and send the results back to a central computer, where analysis would be done. Some  
392 simplified results, such as the percentage of fluorescent particles of biological origin, might be  
393 returned to the volunteer measurer to stimulate and maintain their interest. Or, a cloud-computer  
394 may allow spectra from individual particles to be clustered and compared with a database of  
395 spectral standards for coarse-level discrimination (Pan et al., 2012; Pinnick et al., 2013;  
396 Robinson et al., 2013). Citizen scientist-assisted collection of data about fluorescent aerosol  
397 particles using this technique could help change the face of this area of science by acquiring  
398 orders of magnitude more data points in time and space than are currently available.

399  
400 Although this paper has emphasized the applications of the instrument for acquiring spectral  
401 fluorescence of particles, there may occur even more applications for elastic scattering from  
402 particles, which can be obtained using white light illumination as in Figure 2c rather than 2d. The  
403 technique of acquiring spectra from individual particles can perhaps also be applied to the  
404 acquisition of Raman scattering spectra, though this will introduce additional technical  
405 challenges. Recently an instrument for real-time detection of single particles in air by Raman  
406 spectroscopy has been made commercially available (Hill et al., 2015; Ronningen et al., 2014).



407 The instrument described here could be developed in the future to provide Raman spectroscopy  
408 of individual atmospheric particles, with reduced resolution or signal-to-noise, but also with  
409 significantly reduced cost.

## 410 **7. Summary and conclusions**

411 We have described the development of a small, light-weight and low-cost instrument which uses  
412 the principle of a slitless spectrograph to determine both the elastic scattering spectra and  
413 inelastic spectra (such as fluorescence) for each particle in a many-particle collection on a glass  
414 microscope slide or other surface. In addition to a benchtop model composed of standard  
415 microscope parts, we have shown a small instrument as an attachment to a smartphone or other  
416 small digital camera producing data in the form of images that can be sent immediately from  
417 almost any location on the earth to a remote, master computer for analysis. In the case of its  
418 primary intended use, the instrument can provide separate spectral images of fluorescence and  
419 elastic scatter with which a simple count on these two images is sufficient to determine the ratio  
420 of biological particles to total particles. At present, there are no inexpensive, autonomous sensors  
421 available that can estimate the concentration of mold spores or pollen types that can exacerbate  
422 human allergies. The portable version of the instrument may provide a critical leap in the  
423 detection of several types of biological aerosol particles. For example, by differentiating between  
424 chlorophyll-containing pollen and from other pollen types, the detector could provide a quick  
425 quantification of grass-type pollens (i.e. *Ambrosia* or ragweed) that are responsible for many  
426 cases of hay fever and allergenic rhinitis across the world (D'Amato et al., 2007; O'Connor et al.,  
427 2014).

## 428 **Acknowledgements**

429 The authors acknowledge Brason Holt for assistance with laboratory experiments. DRH  
430 acknowledges the C<sub>60</sub> Patent Royalty Fund of the University of Arizona for support. JAH and  
431 BJS acknowledge funding from the University of Denver professional research opportunities for  
432 faculty (PROF) program.  
433

434 **References and links**

435

436 Abell, G. O.: Exploration of the Universe, Holt, Rinehart &amp; Winston of Canada Ltd, 1969.

437 Bohren, C. F. and Huffman, D. R.: Absorption and Scattering of Light By Small Particles, John  
438 Wiley & Sons, New York, NY, 1983.439 Boyain-Goitia, A. R., Beddows, D. C. S., Griffiths, B. C., and Telle, H. H.: Single-pollen  
440 analysis by laser-induced breakdown spectroscopy and Raman microscopy, Applied Optics, 42,  
441 6119-6132, 2003.442 Cheng, J., Liu, Y., Cheng, X., He, Y., and Yeung, E. S.: Real Time Observation of Chemical  
443 Reactions of Individual Metal Nanoparticles with High-Throughput Single Molecule Spectral  
444 Microscopy, Anal. Chem., 82, 8744-8749, 2010.445 D'Amato, G., Cecchi, L., Bonini, S., Nunes, C., Annesi-Maesano, I., Behrendt, H., Liccardi, G.,  
446 Popov, T., and van Cauwenberge, P.: Allergenic pollen and pollen allergy in Europe, Allergy,  
447 62, 976-990, 2007.448 Després, V. R., Huffman, J. A., Burrows, S. M., Hoose, C., Safatov, A. S., Buryak, G. A.,  
449 Fröhlich-Nowoisky, J., Elbert, W., Andreae, M. O., Pöschl, U., and Jaenicke, R.: Primary  
450 Biological Aerosol Particles in the Atmosphere: A Review, Tellus Series B-Chemical and  
451 Physical Meteorology, 64, 15598, 2012.452 Douwes, J., Thorne, P., Pearce, N., and Heederik, D.: Bioaerosol health effects and exposure  
453 assessment: Progress and prospects, Annals of Occupational Hygiene, 47, 187-200, 2003.454 Foot, V. E., Kaye, P. H., Stanley, W. R., Barrington, S. J., Gallagher, M., and Gabey, A.: Low-  
455 cost real-time multi-parameter bio-aerosol sensors, Proceedings of the SPIE - The International  
456 Society for Optical Engineering, 7116, 711601, 2008.457 Gabey, A. M., Gallagher, M. W., Whitehead, J., Dorsey, J. R., Kaye, P. H., and Stanley, W. R.:  
458 Measurements and comparison of primary biological aerosol above and below a tropical forest  
459 canopy using a dual channel fluorescence spectrometer, Atmospheric Chemistry and Physics, 10,  
460 4453-4466, 2010.461 Hairston, P. P., Ho, J., and Quant, F. R.: Design of an instrument for real-time detection of  
462 bioaerosols using simultaneous measurement of particle aerodynamic size and intrinsic  
463 fluorescence, Journal of Aerosol Science, 28, 471-482, 1997.464 Hale, G. E. and Wadsworth, F. L. O.: The Modern Spectroscope. XIX. The Objective  
465 Spectroscope, The Astrophysical Journal, 4, 54, 1896.466 Healy, D. A., Huffman, J. A., O'Connor, D. J., Pohlker, C., Poschl, U., and Sodeau, J. R.:  
467 Ambient measurements of biological aerosol particles near Killarney, Ireland: a comparison  
468 between real-time fluorescence and microscopy techniques, Atmospheric Chemistry and Physics,  
469 14, 8055-8069, 2014.



- 470 Hernandez, M., Perring, A., McCabe, K., Kok, G., Granger, G., and Baumgardner, D.:  
471 Composite Catalogues of Optical and Fluorescent Signatures Distinguish Bioaerosol Classes,  
472 Atmos. Meas. Tech. Discuss., 2016, 1-17, 2016.
- 473 Hill, S. C., Doughty, D., and Wetmore, A.: Raman Spectra of Individual Particles for  
474 Characterization of Atmospheric Particles, 34th Annual Conference of the American Association  
475 of Aerosol Research (AAAR), Minneapolis, MN, 2015.
- 476 Hill, S. C., Mayo, M. W., and Chang, R. K.: Fluorescence of Bacteria, Pollens, and Naturally  
477 Occurring Airborne Particles: Excitation/Emission Spectra. Laboratory, A. R. (Ed.), Adelphi,  
478 MD, 2009.
- 479 Huffman, J. A., Prenni, A. J., DeMott, P. J., Pöhlker, C., Mason, R. H., Robinson, N. H.,  
480 Fröhlich-Nowoisky, J. F., Tobo, Y., Després, V., Garcia, E., Gochis, D. J., Harris, E., Müller-  
481 Germann, I., Ruzene, C., Schmer, B., Sinha, B., Day, D. A., Andreae, M. O., Jimenez, J. L.,  
482 Gallagher, M., Kreidenweis, S. M., Bertram, A. K., and Pöschl, U.: High concentrations of  
483 biological aerosol particles and ice nuclei during and after rain, *Atmospheric Chemistry and  
484 Physics*, 13, 6151-6164, 2013.
- 485 Huffman, J. A., Sinha, B., Garland, R. M., Snee-Pollmann, A., Gunthe, S. S., Artaxo, P., Martin,  
486 S. T., Andreae, M. O., and Poeschl, U.: Size distributions and temporal variations of biological  
487 aerosol particles in the Amazon rainforest characterized by microscopy and real-time UV-APS  
488 fluorescence techniques during AMAZE-08, *Atmospheric Chemistry and Physics*, 12, 11997-  
489 12019, 2012.
- 490 Huffman, J. A., Treutlein, B., and Pöschl, U.: Fluorescent biological aerosol particle  
491 concentrations and size distributions measured with an Ultraviolet Aerodynamic Particle Sizer  
492 (UV-APS) in Central Europe, *Atmospheric Chemistry and Physics*, 10, 3215-3233, 2010.
- 493 Jenkins, F. A. and White, H. E.: *Fundamentals of optics*, Tata McGraw-Hill Education, 1957.
- 494 Kaye, P. H., Stanley, W. R., Hirst, E., Foot, E. V., Baxter, K. L., and Barrington, S. J.: Single  
495 particle multichannel bio-aerosol fluorescence sensor, *Optics Express*, 13, 3583-3593, 2005.
- 496 Kiselev, D., Bonacina, L., and Wolf, J.-P.: Individual bioaerosol particle discrimination by multi-  
497 photon excited fluorescence, *Optics Express*, 19, 24516-24521, 2011.
- 498 Lakowicz, J. R.: *Principles of Fluorescence Spectroscopy*, Springer, 2010.
- 499 Manninen, A., Putkiranta, M., Rostedt, A., Saarela, J., Laurila, T., Marjamaki, M., Keskinen, J.,  
500 and Hernberg, R.: Instrumentation for measuring fluorescence cross sections from airborne  
501 microsized particles, *Applied Optics*, 47, 110-115, 2008.
- 502 Maxwell, K. and Johnson, G. N.: Chlorophyll fluorescence—a practical guide, *Journal of  
503 Experimental Botany*, 51, 659-668, 2000.
- 504 Möhler, O., DeMott, P. J., Vali, G., and Levin, Z.: Microbiology and atmospheric processes: the  
505 role of biological particles in cloud physics, *Biogeosciences*, 4, 1059-1071, 2007.



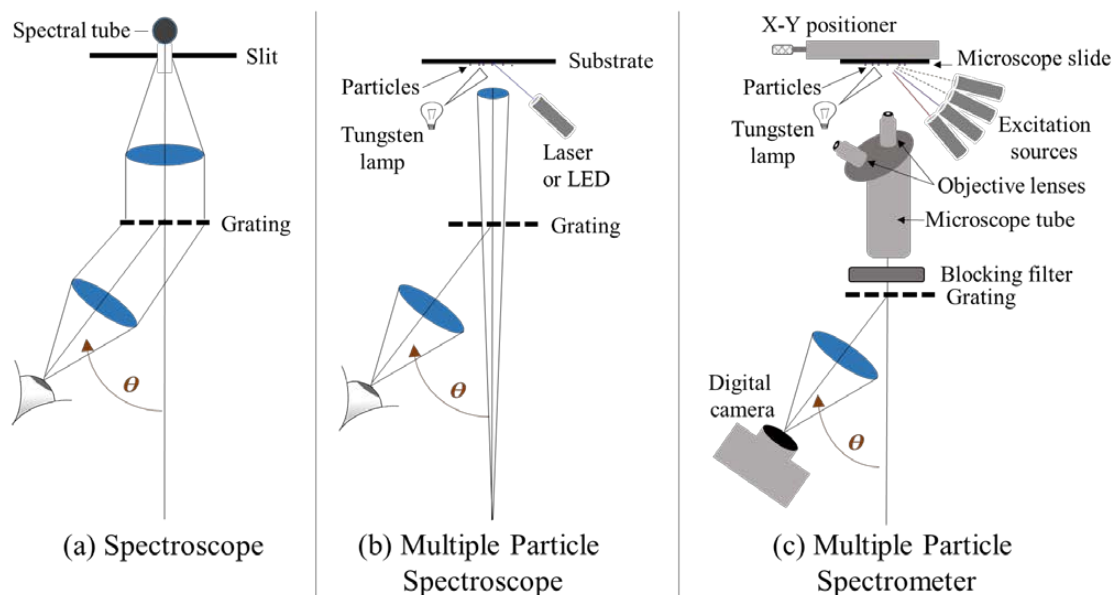
- 506 Morris, C. E., Conen, F., Huffman, J. A., Phillips, V., Pöschl, U., and Sands, D. C.:  
507 Bioprecipitation: a feedback cycle linking Earth history, ecosystem dynamics and land use  
508 through biological ice nucleators in the atmosphere, *Global Change Biology*, 20, 341-351, 2014.
- 509 O'Connor, D. J., Iacopino, D., Healy, D. A., O'Sullivan, D., and Sodeau, J. R.: The intrinsic  
510 fluorescence spectra of selected pollen and fungal spores, *Atmospheric Environment*, 45, 6451-  
511 6458, 2011.
- 512 O'Connor, D. J., Lovera, P., Iacopino, D., O'Riordan, A., Healy, D. A., and Sodeau, J. R.: Using  
513 spectral analysis and fluorescence lifetimes to discriminate between grass and tree pollen for  
514 aerobiological applications, *Analytical Methods*, 6, 1633-1639, 2014.
- 515 Pan, Y.-L., Hill, S. C., Pinnick, R. G., House, J. M., Flagan, R. C., and Chang, R. K.: Dual-  
516 excitation-wavelength fluorescence spectra and elastic scattering for differentiation of single  
517 airborne pollen and fungal particles, *Atmospheric Environment*, 45, 1555-1563, 2011.
- 518 Pan, Y.-L., Huang, H., and Chang, R. K.: Clustered and integrated fluorescence spectra from  
519 single atmospheric aerosol particles excited by a 263- and 351-nm laser at New Haven, CT, and  
520 Adelphi, MD, *Journal of Quantitative Spectroscopy & Radiative Transfer*, 113, 2213-2221,  
521 2012.
- 522 Pan, Y. L., Hartings, J., Pinnick, R. G., Hill, S. C., Halverson, J., and Chang, R. K.: Single-  
523 particle fluorescence spectrometer for ambient aerosols, *Aerosol Sci. Technol.*, 37, 628-639,  
524 2003.
- 525 Pan, Y. L., Hill, S. C., Pinnick, R. G., Huang, H., Bottiger, J. R., and Chang, R. K.: Fluorescence  
526 spectra of atmospheric aerosol particles measured using one or two excitation wavelengths:  
527 Comparison of classification schemes employing different emission and scattering results, *Optics*  
528 *Express*, 18, 12436-12457, 2010.
- 529 Perring, A. E., Schwarz, J. P., Baumgardner, D., Hernandez, M. T., Spracklen, D. V., Heald, C.  
530 L., Gao, R. S., Kok, G., McMeeking, G. R., McQuaid, J. B., and Fahey, D. W.: Airborne  
531 observations of regional variation in fluorescent aerosol across the United States, *J. Geophys.*  
532 *Res.-Atmos.*, 120, 1153-1170, 2015.
- 533 Pinnick, R. G., Fernandez, E., Rosen, J. M., Hill, S. C., Wang, Y., and Pan, Y. L.: Fluorescence  
534 spectra and elastic scattering characteristics of atmospheric aerosol in Las Cruces, New Mexico,  
535 USA: Variability of concentrations and possible constituents and sources of particles in various  
536 spectral clusters, *Atmospheric Environment*, 65, 195-204, 2013.
- 537 Pöhlker, C., Huffman, J. A., Förster, J.-D., and Pöschl, U.: Autofluorescence of atmospheric  
538 bioaerosols: spectral fingerprints and taxonomic trends of pollen, *Atmospheric Measurement*  
539 *Techniques*, 13, 3369-3392, 2013.
- 540 Pöhlker, C., Huffman, J. A., and Pöschl, U.: Autofluorescence of atmospheric bioaerosols -  
541 fluorescent biomolecules and potential interferences, *Atmospheric Measurement Techniques*, 5,  
542 37-71, 2012.



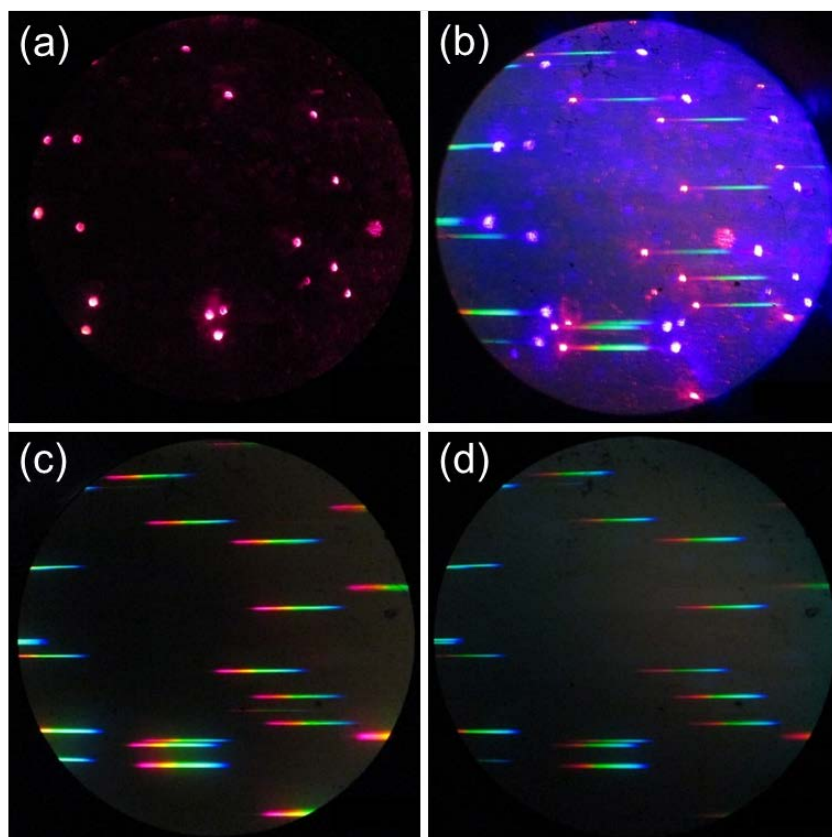
- 543 Pöschl, U., Martin, S. T., Sinha, B., Chen, Q., Gunthe, S. S., Huffman, J. A., Borrmann, S.,  
544 Farmer, D. K., Garland, R. M., Helas, G., Jimenez, J. L., King, S. M., Manzi, A., Mikhailov, E.,  
545 Pauliquevis, T., Petters, M. D., Prenni, A. J., Roldin, P., Rose, D., Schneider, J., Su, H., Zorn, S.  
546 R., Artaxo, P., and Andreae, M. O.: Rainforest Aerosols as Biogenic Nuclei of Clouds and  
547 Precipitation in the Amazon, *Science*, 329, 1513-1516, 2010.
- 548 Pöschl, U. and Shiraiwa, M.: Multiphase Chemistry at the Atmosphere–Biosphere Interface  
549 Influencing Climate and Public Health in the Anthropocene, *Chemical Reviews*, 115, 4440-4475,  
550 2015.
- 551 Rasband, W.: ImageJ, US National Institutes of Health, Bethesda, Maryland, USA, <http://imagej.nih.gov/ij/>, 2012, 1997.
- 553 Robinson, N. H., Allan, J. D., Huffman, J. A., Kaye, P. H., Foot, V. E., and Gallagher, M.:  
554 Cluster analysis of WIBS single-particle bioaerosol data, *Atmospheric Measurement Techniques*,  
555 6, 337-347, 2013.
- 556 Ronningen, T., Schuetter, J., Wightman, J., and Murdock, A.: Raman spectroscopy for biological  
557 identification, *Biological Identification: DNA Amplification and Sequencing, Optical Sensing,*  
558 *Lab-On-Chip and Portable Systems*, 2014. 313, 2014.
- 559 Saari, S., Reponen, T., and Keskinen, J.: Performance of Two Fluorescence-Based Real-Time  
560 Bioaerosol Detectors: BioScout vs. UVAPS, *Aerosol Science and Technology*, 48, 371-378,  
561 2014.
- 562 Saari, S., Reponen, T., and Keskinen, J.: Performance of Two Fluorescence-Based Real-Time  
563 Bioaerosol Detectors: BioScout vs. UVAPS, *Aerosol Sci. Technol.*, 48, 371-378, 2013.
- 564 Schumacher, C. J., Pöhlker, C., Aalto, P., Hiltunen, V., Petäjä, T., Kulmala, M., Pöschl, U., and  
565 Huffman, J. A.: Seasonal cycles of fluorescent biological aerosol particles in boreal and semi-  
566 arid forests of Finland and Colorado, *Atmos. Chem. Phys.*, 13, 11987-12001, 2013.
- 567 Sivaprakasam, V., Huston, A. L., Scotto, C., and Eversole, J. D.: Multiple UV wavelength  
568 excitation and fluorescence of bioaerosols, *Optics Express*, 12, 4457-4466, 2004.
- 569 Sivaprakasam, V., Pletcher, T., Tucker, J. E., Huston, A. L., McGinn, J., Keller, D., and  
570 Eversole, J. D.: Classification and selective collection of individual aerosol particles using laser-  
571 induced fluorescence, *Applied Optics*, 48, B126-B136, 2009.
- 572 Xiong, B., Zhou, R., Hao, J., Jia, Y., He, Y., and Yeung, E. S.: Highly sensitive sulphide  
573 mapping in live cells by kinetic spectral analysis of single Au-Ag core-shell nanoparticles, *Nat*  
574 *Commun.*, 4, 1708, 2013.  
575



576 **Figures**

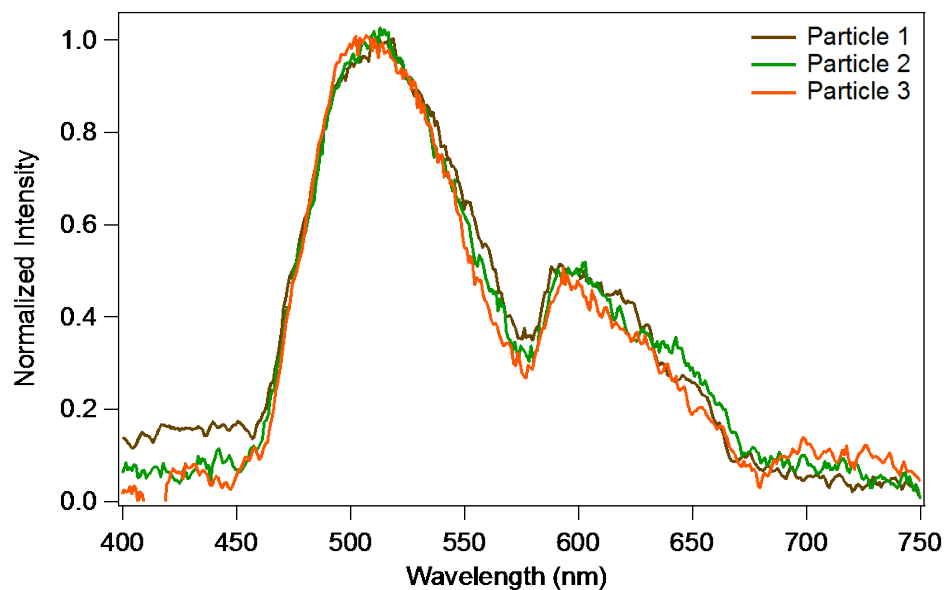


577  
578 **Figure 1:** Three-stage progression of spectrometer. (a) Spectroscope, as often utilized in student  
579 laboratories. (b) Multiple particle spectroscope. (c) Multiple particle spectrometer (introduced  
580 here).

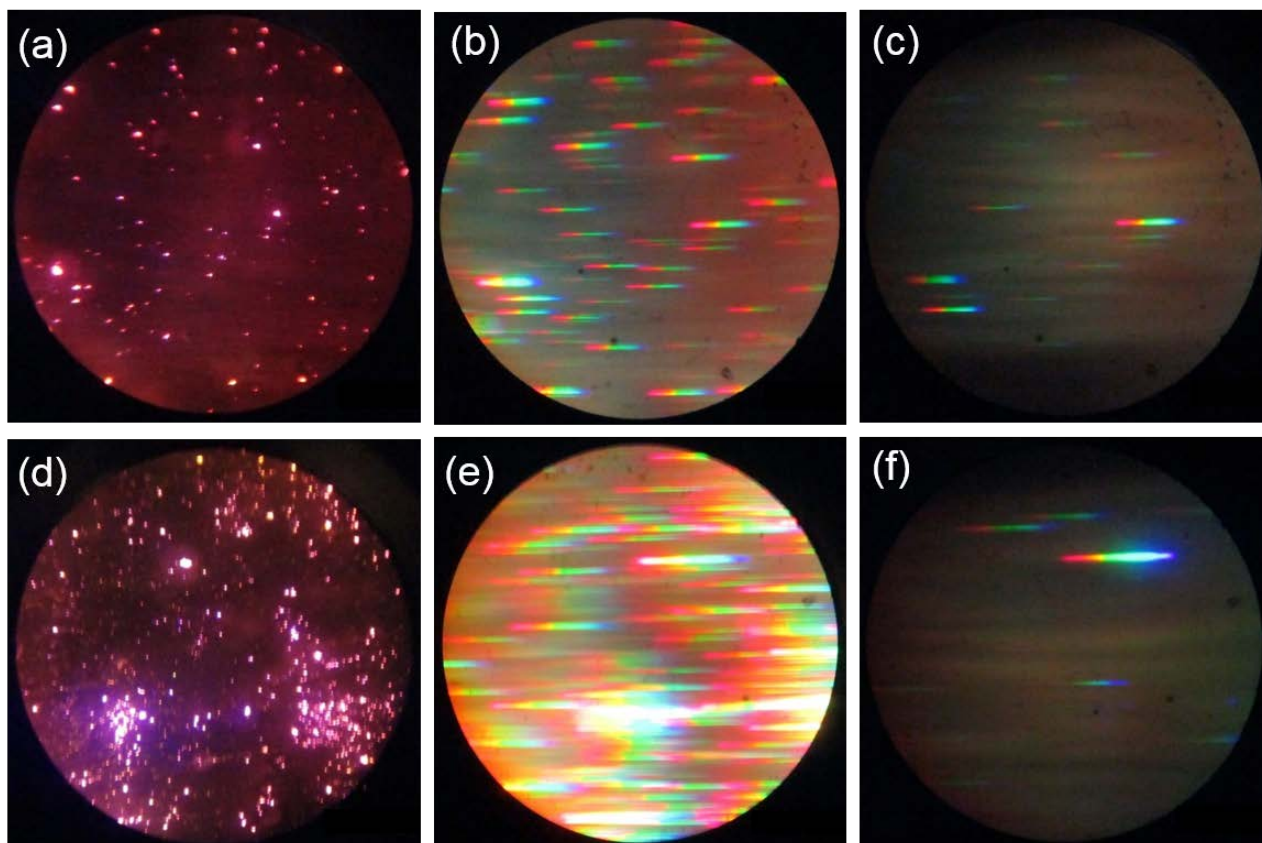


581  
582  
583  
584  
585  
586  
587  
588  
589  
590

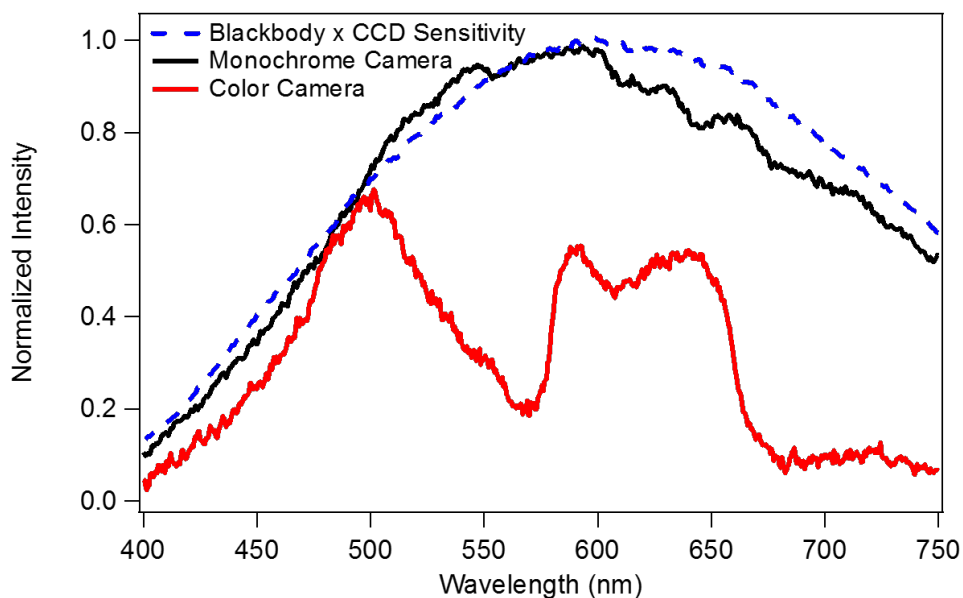
**Figure 2:** Four-panel progression of images acquired for a given scene of paper mulberry pollen particles collected onto a glass microscope slide. Scale is the same in each figure, with each horizontal swath of color approximately 10  $\mu\text{m}$  in height. (a) Dark field image of particles illuminated by monochromatic red laser light ( $\theta = 0$ ). (b) Particles illuminated with both violet (405 nm) and red (650 nm) diode lasers. Fluorescent spectra of individual particles showing image taken without use of blocking filter. (c) White light illumination with tungsten filament bulb. (d) Fluorescent emission with excitation from violet diode laser, but using blocking filter to remove violet laser point.



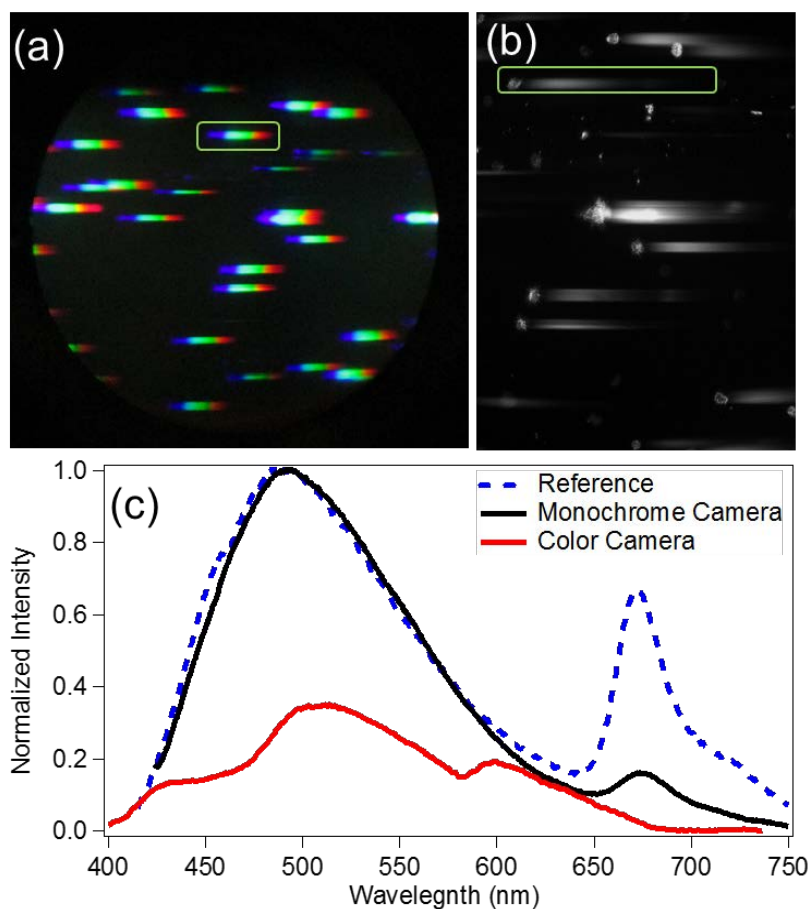
591  
592 **Figure 3:** Fluorescent spectra of three individual paper mulberry pollen particles (*Broussonetia*  
593 *payrifera*) illuminated by 405 nm diode laser (Fig. 2d). Emission wavelength was calibrated  
594 using 405 nm and 650 nm laser points (Fig. 2b). All spectra were normalized to 1.0 maximum  
595 peak height.



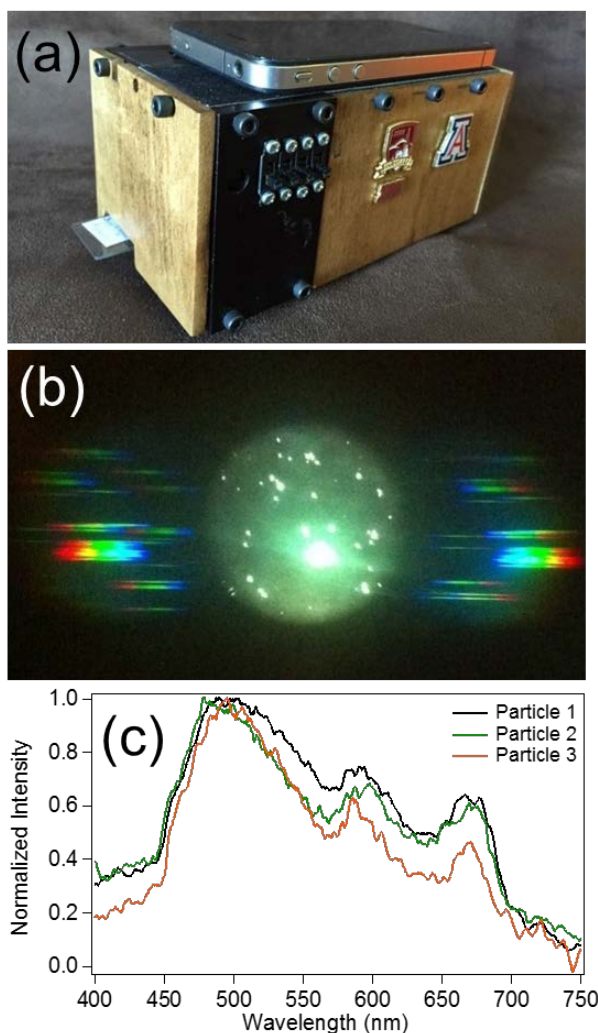
596  
597 **Figure 4:** Images showing minority of fluorescent particles amidst large quantity of other  
598 particles. (a-c; top panels) outdoor ambient particles collected via natural settling onto  
599 microscope slide. (d-f; bottom panels) ground optical fused quartz particles. First column (a,d)  
600 shows conventional micrograph images ( $\theta = 0$ ) illuminated with red laser light. Second column  
601 (b,e) shows white light scattering spectra after illumination of same scene with polychromatic  
602 light from tungsten source. Third column (c,f) shows fluorescent spectra after illumination of  
603 same scene with 405 nm diode laser and blocking filter in place.



604  
605 Figure 5: Comparison of white light scattering from ground sodium chloride (NaCl) particle  
606 detected by color (solid red) and monochrome (solid black) cameras. Reference spectrum  
607 (dashed blue) shows calculated blackbody radiator at 3000 K multiplied by CCD sensitivity  
608 curve as an estimate of light intensity as a function of wavelength expected at detector. Red  
609 curve was normalized to 1.0 and then scaled down by an arbitrary value to show reduced  
610 emission intensity above 500 nm.



611  
612 **Figure 6:** Spectral images and associated spectra for individual particles of Kentucky bluegrass  
613 (*Poa pratensis*) pollen. Both images show fluorescence of particles illuminated by 405 nm diode  
614 laser and utilizing 420 nm long-pass blocking filter. (a) Color camera detection. (b) Black-and-  
615 white camera detection. (c) Spectra of one particle from each image (boxed particle from a,b  
616 shown). Reference spectrum (dashed line) from microplate reader spectrofluorometer showing  
617 bulk average of ~5 mg of material. Spectra from monochrome camera and reference technique  
618 normalized to peak height of 1.0. Spectrum from color camera arbitrarily scaled to show reduced  
619 intensity of collection compared to monochrome camera.



620  
621 **Figure 7:** Smartphone spectrofluorometer prototype. (a) Photograph of iPhone spectrometer. (b)  
622 Standard micrograph (dots) and fluorescent swaths (left and right portions) collected as single  
623 image with iPhone 5s shown in panel (a). Particles are Kentucky bluegrass pollen (*Poa*  
624 *pratensis*) (c) Spectra of three of the smaller particles from panel (b), normalized to peak height  
625 of 1.0.